

Investigation of $\text{Ca}_{12}\text{Al}_{14}\text{O}_{33}$ Mayenite for hydration/dehydration thermochemical energy storage

Abdelali Zaki^{1,*}, Andrea Gutierrez^{2,*}, Matthias Schmidt³, Daniel Bielsa¹, Marc Linder², Abdessamad Faik^{1,4}

¹ CIC Energigune, Albert Einstein 48, 01510 Miñano (Álava), Spain

² German Aerospace Center –DLR e.V., Institute of Engineering Thermodynamics, Pfaffenwaldring 38, 70569 Stuttgart, Germany

³ German Aerospace Center –DLR e.V., Institute of Engineering Thermodynamics, Linder Höhe, 51147 Köln, Germany

⁴ Materials Science and Nano-engineering, Mohammed VI Polytechnic University, Lot 660-Hay Moulay Rachid, Ben Guerir, Morocco

* Corresponding authors: Phone: (+34) 945 297 108, e-mail: azaki@cicenergigune.com; Phone: (+49) 711 6862 8236 e-mail: Andrea.GutierrezRojas@dlr.de

Abstract

Thermal energy storage using a reversible chemical reaction is a key parameter for increasing the storage capacity especially for medium and high temperature applications. The reversible hydration/dehydration reaction of calcium hydroxide $\text{Ca}(\text{OH})_2$ to calcium oxide CaO is among the most investigated system due to its reaction cyclability and interesting operating temperature above $450\text{ }^\circ\text{C}$ suitable for high temperature applications. However, the indicated reaction temperature was considered too high for some industrial applications which limit a further development of thermal energy storage technologies using this promising reaction system. In this regard, the material development is a key point to broaden the application of sustainable technologies. In this work, the investigation of Mayenite with general formula $\text{Ca}_{12}\text{Al}_{14}\text{O}_{33}$ as a thermochemical energy storage material was conducted. Thereby, it was confirmed the possibility of the pair “ $\text{Ca}_{12}\text{Al}_{14}\text{O}_{12}(\text{OH})_{42}$ ”/ $\text{Ca}_{12}\text{Al}_{14}\text{O}_{33}$ to store and release the heat through chemical reaction thanks to a novel activation process of the pristine Mayenite that is presented for the first time in this work. This study might help to identify new pairs based on materials that have already been classified as inactive for the hydration/dehydration reaction. In addition, it was found that the hydration reaction temperature of “ $\text{Ca}_{12}\text{Al}_{14}\text{O}_{12}(\text{OH})_{42}$ ”/ $\text{Ca}_{12}\text{Al}_{14}\text{O}_{33}$ pair of 228°C is much lower compared to that of $\text{CaO}/\text{Ca}(\text{OH})_2$.

Keywords: Thermochemical heat storage; Gas-solid reaction; Hydration/dehydration reaction; Calcium aluminates; Mayenite.

1. Introduction

The use of renewable energy sources nowadays is vital in order to decrease the consumption of fossil resources and to decrease the carbon dioxide emissions partly responsible for the greenhouse effect. Energy storage is a promising solution which allows adjusting the time-discrepancy between supply and demand of energy. It is mainly applied for the utilization of intermittent energy sources, such as solar energy, variable energy load, and excessive energy uses in industrial process that would be wasted. Energy can be stored in different ways, such as mechanical energy, electric energy, chemical energy and thermal energy, where the last one is potentially capable of improving the efficiency of the concentrate solar power (CSP) plants and upgrade of the recovered low grade heat in industrial processes, among other applications[1].

There are three well known methods for thermal energy storage (TES), sensible, latent and chemical. The sensible and latent TES are the most developed technologies, where the first system stores the heat by a temperature change of the storage material; while the second system stores the heat by a phase change of the storage material. However, the storage density depends, in the first case, on the mass, the specific heat capacity of the storage medium and the applied temperature change [2]. The least developed TES technology is the thermochemical storage, which is based on the mass, the temperature range and the enthalpy of the reversible chemical reaction. This technology presents the highest theoretical energy density compared to that of sensible and latent heat storages [3].

In this perspective, thermochemical storage is considered as a very promising technology not only due to its higher theoretical storage energy, but also for the possibility of a long-term storage applications, as the reaction products can be stored at room temperature without any significant energy losses [4,5]. In the literature, different types of reversible reactions have been considered where the solid-gas reactions were extensively investigated due to some extra advantages such as easy separation of the reactants and, the dependence between the equilibrium temperature and gas pressure, which allows adjusting the reaction temperature

of the system. For this purpose, many types of solid-gas reactions have been studied such as reduction/oxidation[6–8], decarbonation/carbonation[9,10] and hydration/dehydration[11–13]. Among these systems, hydration/dehydration systems present the most interesting temperature level that is suitable for high temperature TES applications such as those in the current CSP technologies and some industrial processes[14–17]. In this sense, a suitable material is needed that is able not only to run the endothermic dehydration reaction, by absorbing heat when is available, but also to conduct the reversible exothermic hydration reaction by fully releasing absorbed heat when is needed. The most widely investigated system is the calcium hydroxide/calcium oxide $\text{Ca(OH)}_2/\text{CaO}$ pair following the reversible hydration/dehydration reaction (eq. 1).



This system has been selected as the best candidate for its suitable equilibrium temperature (450 °C – 500 °C), the low cost and non-toxicity of the materials, relatively high energy density (450 kW_h/m^3), fast kinetics, reversibility and cycling stability [12,18]. Most of the studies have been focused on explaining the reaction mechanisms and to evaluate the impact of the physical bulk properties of the material on the operation characteristics of the storage systems[11]. Those works were focused on studying the reaction from a thermodynamic perspective by using small sample masses in thermogravimetric apparatus and the development of simulation models to understand the behavior of the materials [19,20]. Other research activities aimed to enhance the reaction rate by improving the flowability of the material by the addition of nanoparticles as spacers or by the impregnation of calcium hydroxide into inert materials forming robust porous matrices [21]. In addition, some research groups were devoted on mechanical cycling stability studies of the materials by means of encapsulation of the storage material (calcium hydroxide) in a permeable shell.[3] Recently, a step forward had been made in order to investigate the behavior of the system in large scale in fixed bed configuration[22] and moving bed concept [20]. Despite those efforts the technology is still under development and in an early research state.

One major drawback revealed by the experimental investigations is, that even when the system is operated at very low vapor pressures (e. g. 10 kPa), a minimum charging temperature of 450 °C is required in order to achieve technically relevant charging powers.

The high charging temperature limits the efficient application of the storage system into the process. The main advantage of the new reaction pair proposed here is the possibility to adjust the reaction temperature. This offers the feasibility to apply it to other applications than power tower CSP technologies that are operated at lower heat transfer fluid and energy storage medium temperatures such as the parabolic troughs and linear Fresnel concepts or even to thermal storage applications in e.g. process industry. Hence, a lower dehydration temperature of the reaction would greatly enhance the efficient process integration of the storage system for various applications [22,23]. Therefore, more efforts are required in order to develop new materials with equilibrium temperatures adapted to the final applications. In this regard, the investigation of new materials of magnesium hydroxide - porous matrix composites was conducted aiming to overcome the aforementioned limitations [24].

Mayenite has been widely used as a major constituent of calcium aluminate cements. Furthermore, this material has attracted the attention of the scientific and technological communities to be used as a transparent conductive oxide, as a catalyst for the combustion of volatile organic compounds or as an ionic conductor[25]; but, to the best of our knowledge, this is the first work dealing with the valorization of that material for thermochemical energy storage applications. The preparation of the pure $\text{Ca}_{12}\text{Al}_{14}\text{O}_{33}$ material was obtained by Evaporation-Induced Self-Assembly (EISA) method. The crystallographic structure of the material and the size and morphology of the particles were investigated by means of X-ray powder diffraction (XRD) and scanning electron microscopy (SEM), respectively. The simultaneous thermal analysis (STA) was used to investigate the thermophysical characteristics, the equilibrium reaction temperatures, conversion rate and the re-hydration of the material.

2. Techniques and Materials

2.1. Material synthesis

The Evaporation-Induced Self-Assembly (EISA) method [26] was used for the synthesis of mixed calcium/aluminum oxide with the general formula $\text{Ca}_{12}\text{Al}_{14}\text{O}_{33}$. The aluminum isopropoxide $\text{C}_9\text{H}_{21}\text{O}_3\text{Al}$ (98%) and calcium nitrate tetrahydrate $\text{Ca}(\text{NO}_3)_2 \cdot 4\text{H}_2\text{O}$ (98%) are used, as received from Sigma-Aldrich, as aluminum and calcium precursors, respectively. Typically, for 3 g of $\text{Ca}_{12}\text{Al}_{14}\text{O}_{33}$ material preparation, 6.12 g of $\text{C}_9\text{H}_{21}\text{O}_3\text{Al}$ is dissolved in a

pre-mixed solution of 60 mL of ethanol and 4.5 mL HNO₃ (67 wt. %) by vigorous stirring for 1 hour. Then, to this homogenous solution, 6.072 g of Ca (NO₃)₂·4H₂O were added and stirred continuously for another 5 hours. Then, the mixture was dried at the oven at 80°C during 1 day in air under static condition. To study the effect of the calcination temperature on the material crystallinity and particle size, four samples were calcined successively at 600, 800, 1000 and 1100 °C, with a heating/cooling rate of 1 °C/min and a dwell for 10 hours. The thermodynamic behavior of the four samples was investigated in order to investigate the effect of the crystallinity and particle size on the hydration and dehydration processes.

In order to facilitate the understanding of the results the Mayenite samples were identified as shown in **Table 1** and the details about the activation process will be explained later in section 3.

Table 1. Identification of Mayenite samples

Material	T _{calcination} [°C]	Activation status	Label
Mayenite	600	Non-Activated	M-600-NA
		Activated	M-600-A
	800	Non-Activated	M-800-NA
		Activated	M-800-A
	1000	Non-Activated	M-1000-NA
		Activated	M-1000-A
1100	Non-Activated	M-1100-NA	

2.2. Activation process

The samples prepared at 600, 800, 1000 and 1100 °C were initially hydrated using a hydrothermal set-up. However, 100 mg of dry powders were introduced in alumina crucibles, which, then each crucible was introduced in a bottle of Teflon of 250 mL filled with 15 mL of distilled water. The systems were hermetically closed and introduced in a furnace at 170 °C for 30 minutes.

2.3. Structural and morphology characterizations

The X-ray powder diffraction (XRD) and scanning electron microscopy (SEM) were conducted to determine the structural characteristics and the particle size of the samples prepared at 600, 800, 1000 and 1100 °C.

Bruker D8 Advance diffractometer equipped with a LYNXEYE detector using $\text{CuK}_{\alpha 1}$ radiation ($\lambda = 1.5418 \text{ \AA}$) and θ - 2θ geometry was used for XRD analysis. The data were collected at room temperature between 10° and 80° with a step size of 0.02° and a counting time of 8 seconds per step. The Rietveld refinement of the crystallographic structure was performed using the WinPlotr/FullProf package[27]. The peak shape was described by a pseudo-Voigt function, and the background level was modeled using a polynomial function. The refined parameters were: background coefficients, scale factor, lattice constants, atomic positions, isotropic independent atomic displacement parameters, zero shift, peak profile and asymmetry parameters.

The samples were imaged by means of a SEM Quanta 200 FEG operated in high vacuum mode at 30 kV featured with a secondary electron detector (ETD). To perform the SEM analysis, small amount of the powder was placed on a graphite holder using double-sided carbon tape.

2.4. Thermal analysis

Thermogravimetric analysis studies were carried out by using simultaneous thermal analysis (STA409, Netzsch). The measurements were carried out on about 20 mg of the samples placed in an alumina crucible with a volume of 100 μL at a constant heating/cooling rate of 2 K/min. The reversibility of dehydration/hydration reactions and the thermodynamic properties, namely temperatures of dehydration/hydration and cycle stability, were studied using a simultaneous thermal analyzer (STA-449C Jupiter®, Netzsch). The set-up was equipped with a water vapor generator (aDrop, Bronkhort®) and with a water vapor furnace. A thermogravimetric (TG) sample carrier with a thermocouple Type S and an accuracy of $\pm 1 \text{ K}$ was used. Sample sizes of $\sim 6 \text{ mg}$ were measured in Al_2O_3 crucible (3.4 mL). In addition, a thermogravimetric-differential scanning calorimetric (TG-DSC) sample carrier with a thermocouple Type K and an accuracy of $\pm 1 \text{ K}$ was used. With these results the relative enthalpy of dehydration was calculated for each of the materials using $\text{Ca}(\text{OH})_2$ as a reference material. Sample sizes of about $\sim 6 \text{ mg}$ were measured in open platinum crucibles

(95 μL). The accuracy of the thermo-balance was $\pm 0.1 \mu\text{g}$. The absolute pressure inside the furnace was equal to the atmospheric pressure (96 kPa). Nitrogen was used as protective and purges gas with a volume flow for both of 50 N-mL/min. The atmosphere surrounding the sample was kept inert using 100 N-mL/min of nitrogen flow and water vapor. Either pure nitrogen was used or a mix of nitrogen and water vapor in order to obtain different partial pressures of water vapor. Partial vapor pressures of 68 kPa or $96 \text{ kPa} \pm 1 \text{ kPa}$ were set for the samples rehydration. Dynamic experiments were set to study the reversibility of reactions, with heating and cooling rates of 5 K/min and -5 K/min, respectively. The relative enthalpies of dehydration were determined performing also dynamic experiments, with heating rates of 1 K/min. The cycle stability was evaluated at isothermal conditions defined as a function of the temperatures of hydration determined in the previous experiments. Ten cycles of hydration and dehydration were performed alternating inert and humid ($p_{\text{H}_2\text{O}} = 68 \text{ kPa}$) atmosphere.

3. Results and Discussions

3.1. Characterization of the samples.

The final synthesis temperature is a key parameter for obtaining pure samples with different levels of crystallinity and particle size. Figure.1 presents the XRD diffractograms obtained at room temperature for $\text{Ca}_{12}\text{Al}_{14}\text{O}_{33}$ samples calcined at 600, 800, 1000 and 1100 $^{\circ}\text{C}$. The samples prepared at 600 and 800 $^{\circ}\text{C}$ show amorphous nature, where almost no peaks were observed; while, the sample treated at 1000 $^{\circ}\text{C}$ shows almost pure crystalline phase corresponds to Mayenite structure with the presence of small peaks at around 28 $^{\circ}$, 30 $^{\circ}$ and 31 $^{\circ}$ corresponding to unidentified impurities. The sample treated at 1100 $^{\circ}\text{C}$ demonstrates a good crystallinity without the presence of any extra peaks related to some impurities. In order to check the sample purity and the crystallographic information of this material, a Rietveld refinement was conducted using as a starting model the published Mayenite structure [28]. The refinement results are presented in Figure 2, where a good agreement between the experimental and calculated XRD patterns was obtained, which demonstrates the purity of the sample treated at 1100 $^{\circ}\text{C}$.

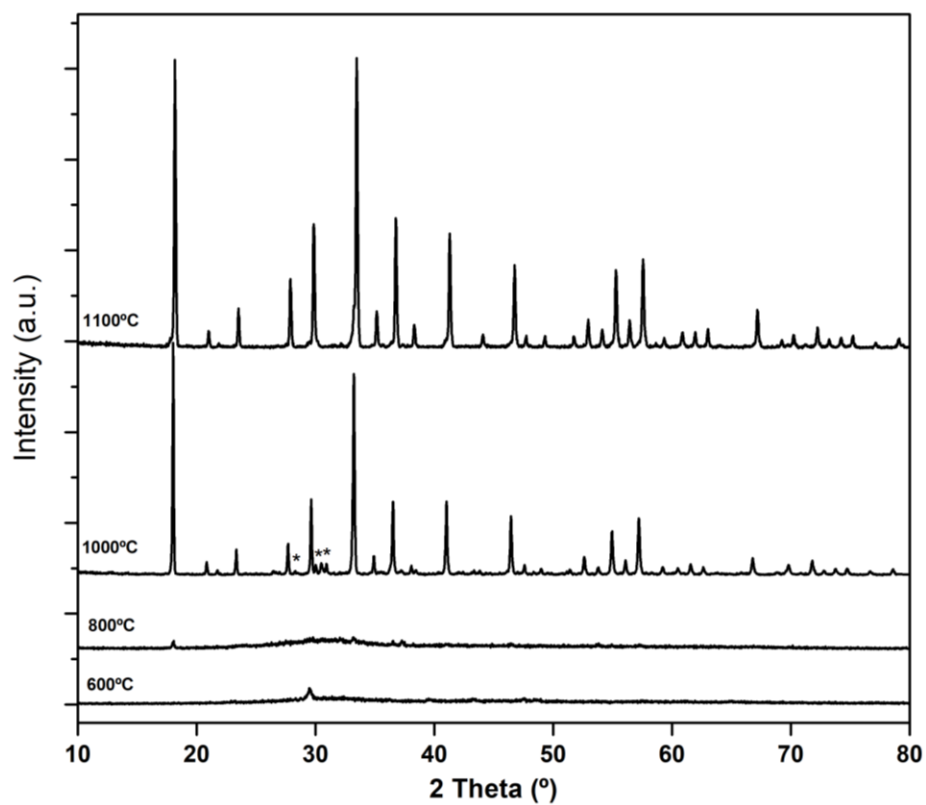


Figure 1. XRD patterns obtained at room temperature for $\text{Ca}_{12}\text{Al}_{14}\text{O}_{33}$ samples prepared at 600, 800, 1000 and 1100 °C. (*) corresponds to unidentified impurities.

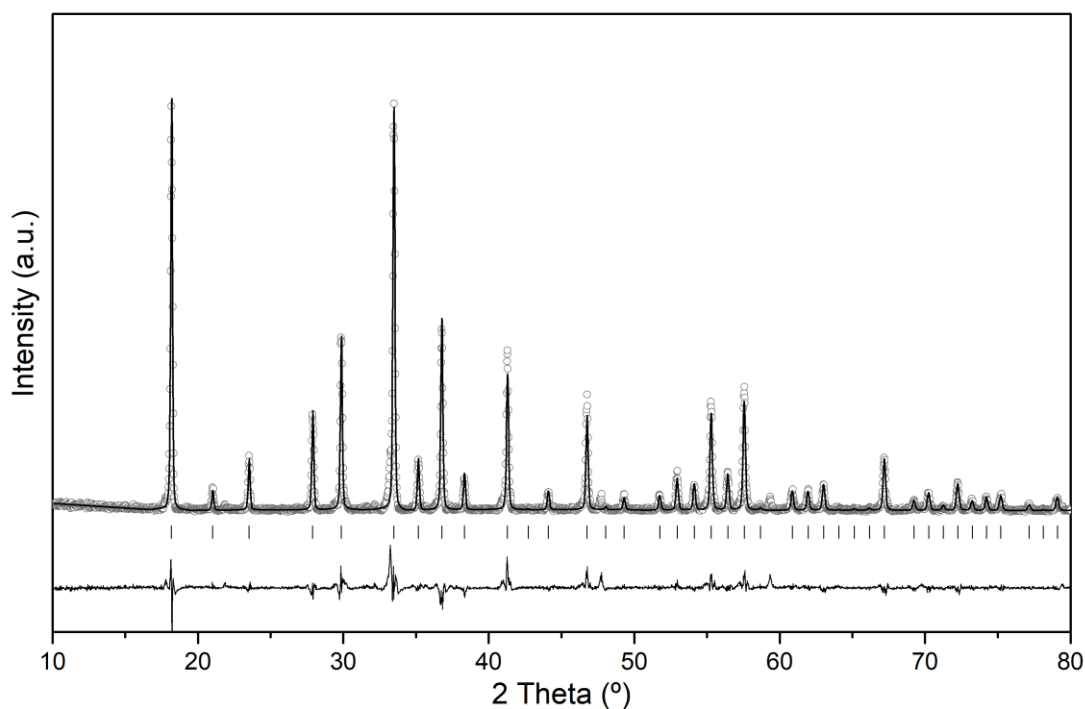


Figure 2. Experimental (symbols) and calculated (line) XRD patterns obtained for $\text{Ca}_{12}\text{Al}_{14}\text{O}_{33}$ prepared at 1100 °C. The bars in the lower part of the graphics represent the Bragg peak positions.

The obtained structure of Mayenite, $\text{Ca}_{12}\text{Al}_{14}\text{O}_{33}$, has a cubic crystal system with the space group I-43d and a lattice parameter constant of 11.982(1) Å, containing two molecules per unit (1720.24(2) Å³). Figure 3a illustrates the Mayenite structure that can be represented as a tri-dimensional network of 12 sub-nanocages, where, each cage is elongated and contains two crystallographic positions for the oxide ion and the two so-called extra-framework oxide ions are randomly distributed in those cages[25,29,30]. The effective diameter of nanocages is ranging between 0.44 nm and 0.56 nm depends on the oxide ion contained inside [25,31]. The extra-framework oxide ions can be replaced by monovalent species, such as OH⁻ group [32]. There is a main difference between the Mayenite which possesses an oxide ion inside the nanocages and the Zeolite structures is the charge polarity of the lattice framework; cationic species are introduced to compensate for the negative charge caused by the substitution of Al³⁺ ion by Si⁴⁺ ion in the Zeolites, which, in this case, does not allow to the oxide ions in the cages to react with water molecules. The Zeolite structure counts with two big cages, α -cage and β -cage with respectively internal diameter of 1.1 nm and 0.8 nm, which, in this case, allows to Zeolite to adsorb a big quantity of water molecules[33]. This difference

leads to an hydration thermodynamics for Mayenite and not to water uptake compared to conventional Zeolite structure.

The hydration reaction can be described as follow:

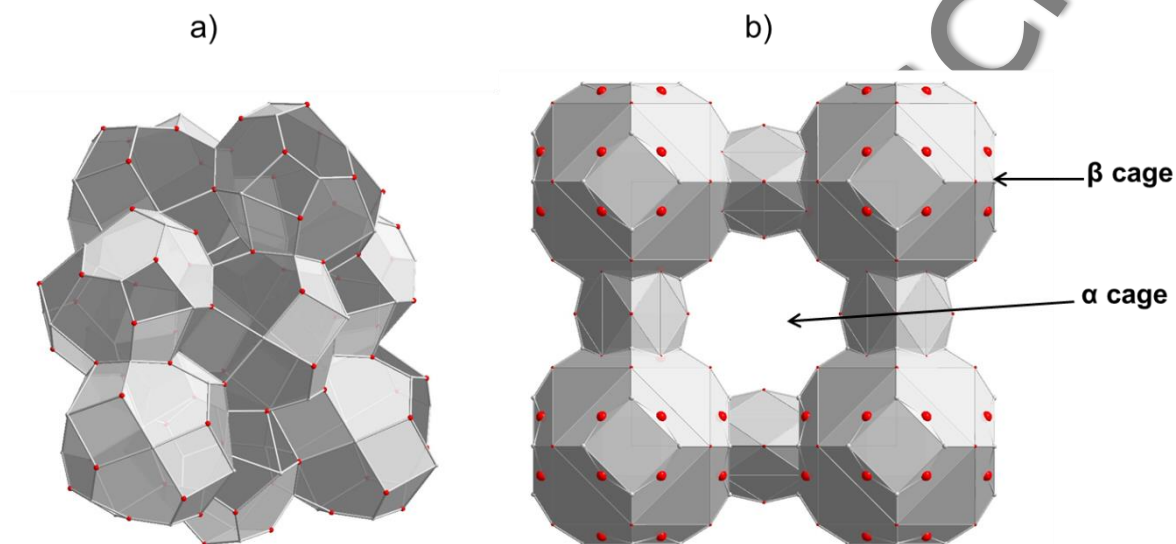


Figure 3. (a) Mayenite crystal structure showing the nanocages. (b) Zeolite crystal structure illustration α -cage and β -cage.

The particle size and morphology of the oxide materials obtained at 600, 800, 1000 and 1100 °C were investigated by SEM analysis. Figure 4 shows the obtained SEM micrographs where a notable increase of the particles size ($\sim 1.5 \mu\text{m}$) was obtained for the sample treated at 1100 °C, while a similar small size (less than 200 nm) was obtained for the rest of the samples. For the material prepared at 600 °C, we observe two types of particles, rods and spherical shape that can be explained by the non-sufficient reaction temperature where the reaction was carried out in order to form the crystalized mixed oxide of Mayenite. The particles morphology becomes more homogeneous for the materials treated at 800, 1000 and 1100 °C, where it was observed that the mixed phase becomes dominant for both samples.

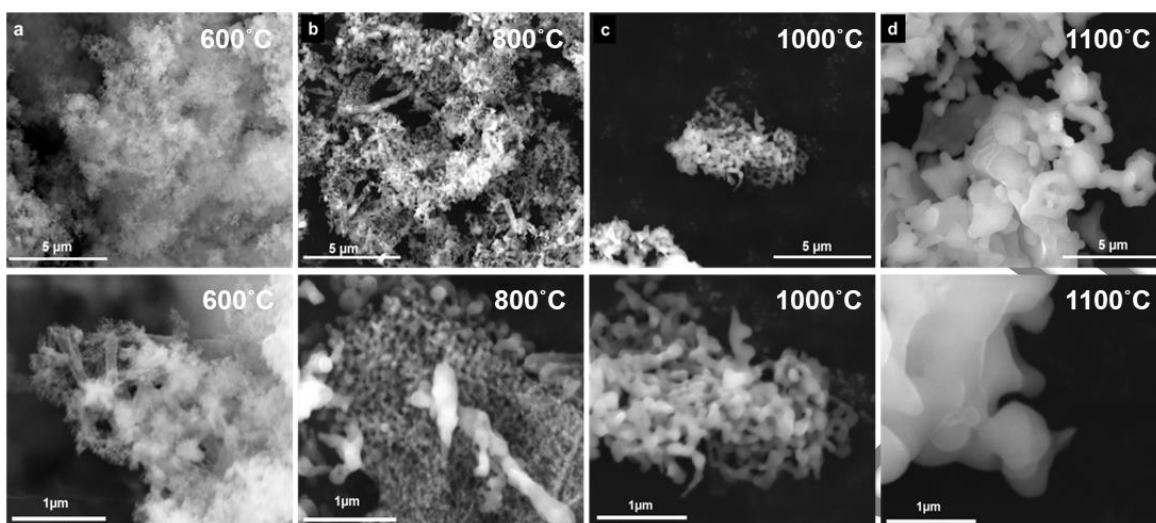


Figure 4. SEM micrographs of $\text{Ca}_{12}\text{Al}_{14}\text{O}_{33}$ prepared at (a) 600, (b) 800, (c) 1000 and (d) 1100 °C.

3.2. Thermal analysis

3.2.1 Activation of the materials

The hydration/dehydration analysis shows that the hydration process of the pristine materials prepared at 1000 and 1100 °C is very hard to be conducted at low partial pressures of water vapor (96 kPa) as shown in Figure 5. In the case of the pristine material prepared at 1100 °C, the sample showed about 2 wt% of chemical reversibility during the first dehydration. However, in the following cycles, this reversibility is slightly higher; reaching up to 2.2 wt% during the last hydration. A similar tendency is observed for the pristine material prepared at 1000 °C. Nevertheless, the mass difference due to the hydration and dehydration of M-1000-NA was more significant from the first cycle in comparison with the M-1100-NA. In the first cycle a chemical reversibility close to 3 wt% was observed. While in the last cycle the chemical reversibility is more than 4.5 wt%, even exceeding the initial mass which corresponds to 100 wt% sample mass. Therefore, and based on the comparison of different analyses it was demonstrated that the hydration process becomes harder when the crystallinity of the material increases. In addition, in the case of the material calcined at 1100 °C, due to the big size of the particles which refers to the high crystallinity of the sample as confirmed by XRD pattern shown in Figure 5, the incorporation of the water molecule becomes more difficult in order to convert the oxide to hydroxide form.

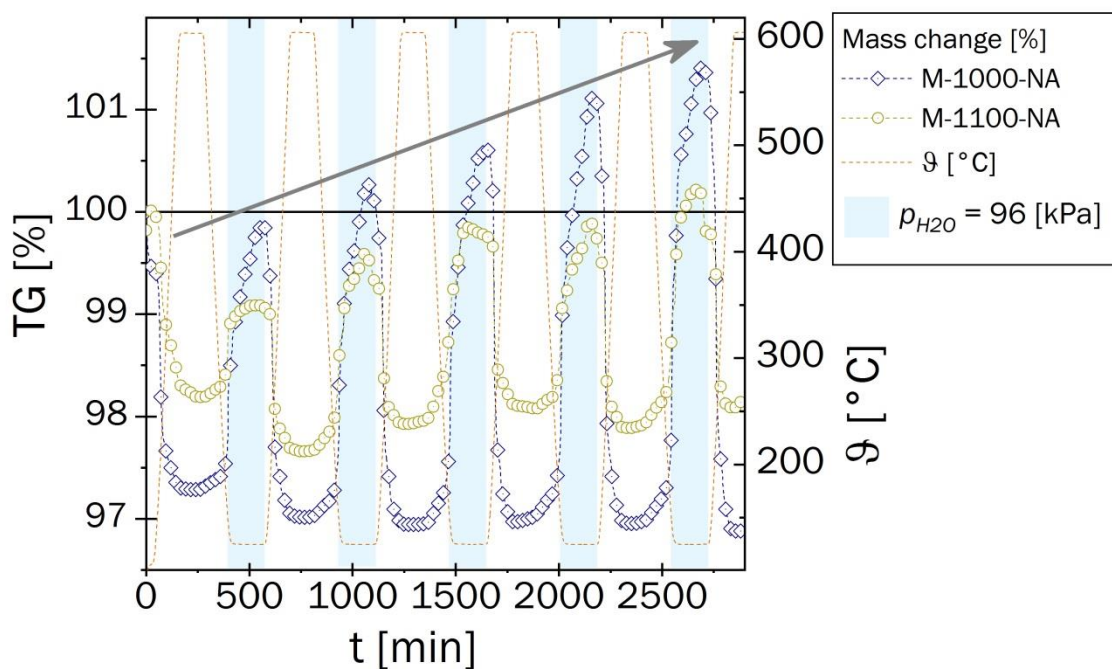


Figure 5. Chemical reversibility over 5 cycles ($p_{H_2O} = 96$ kPa) of Mayenite prepared at 1100 °C and at 1000 °C.

For that reason, we carried out an ex-situ hydration under severe conditions aiming to activate the materials.

Thereafter, the high pressure of water vapor created by a hydrothermal set-up, forces the hydration process for the samples prepared at 600, 800 and 1000 °C and generates a hydration/dehydration reversible behavior for these materials as it was confirmed by thermogravimetric analyses.

The activated samples showed a reversible behavior of hydration/dehydration under operating temperatures between 125°C and 300°C (Figure 6). Which are considerably lower than calcium oxide (CaO), for which theoretical hydration temperatures close to 250°C ($p_{H_2O} < 2$ kPa) and dehydration temperatures close to 380°C ($p_{H_2O} < 1$ kPa) have been previously reported[18]. In addition, the sample prepared at 600°C (M-600-A) showed a continuous mass increase during the isotherm exceeding the initial mass (at $t=0$ min); this could be a consequence of the low temperature of preparation that does not allow the formation of the mixed structured (this was previously mentioned in section 3.1). Therefore, after the first dehydration the anhydrous phase undergoes not only the reaction of

(re)hydration but seems to continuously adsorb water on the surface of the powder sample. In contrast, the other two samples, M-800-A and M-1000-A, reached a constant mass increase during the isotherm. This demonstrates that the reaction has reached equilibrium, and hence, that no higher chemical conversion can be reached under these operating conditions (125°C and $p_{H_2O}=96$ kPa).

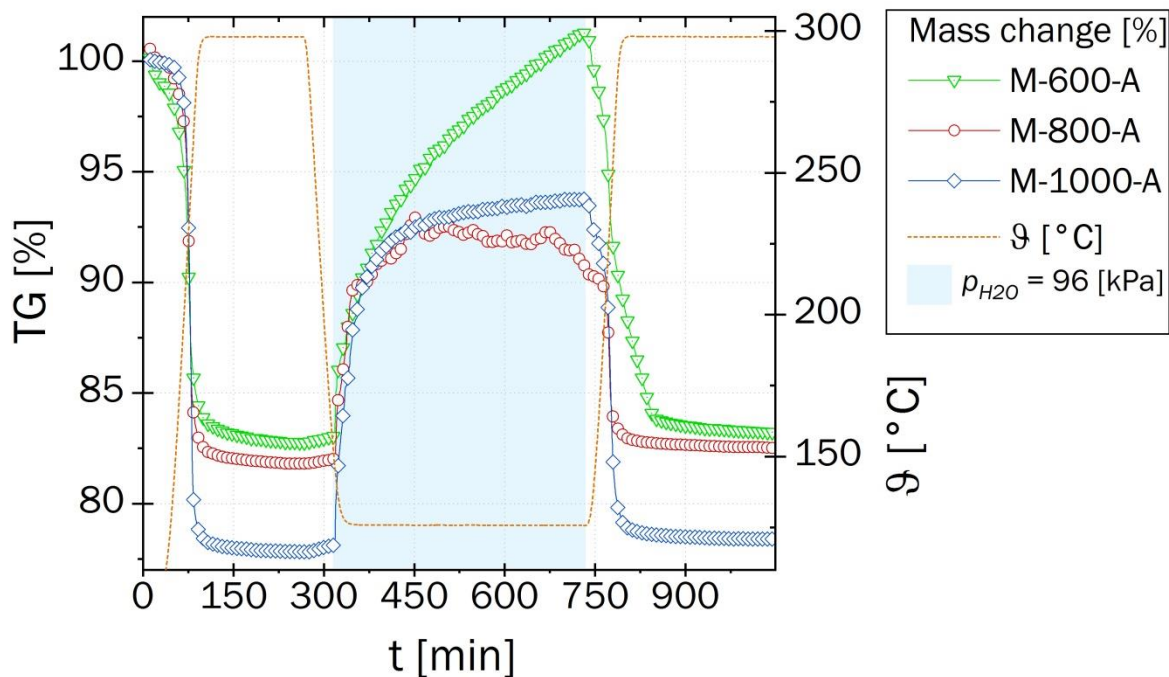


Figure 6. Chemical reversibility of activated samples

However, this new finding might remove huge barriers in order to expand the thermochemical energy storage systems with water vapor to new mixed materials which cannot be considered for that purpose due to their initial inability to react with water molecules (inactive materials). This pre-hydration process is considered as an activation process for the materials to facilitate their further hydration/dehydration cycling.

On the other hand, unsuccessful activation process was obtained for the material prepared at 1100 °C due to the big size particles and the high crystallinity as it is shown in Figure 7 in which, the material prepared at temperature of 1000 °C exhibits a change of the particle

morphology generating hexagonal shape that confirms the formation of the hydrated form.

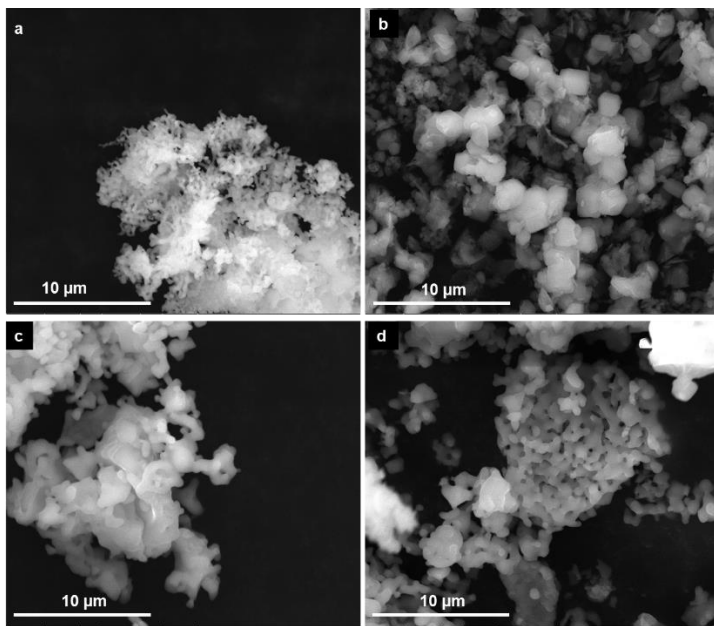


Figure 7. SEM micrographs $\text{Ca}_{12}\text{Al}_{14}\text{O}_{33}$ materials calcined at 1000 °C (a) anhydrous and (b) hydrated; and at 1100 °C (c) anhydrous and (d) hydrated.

3.2.2. Thermodynamic study

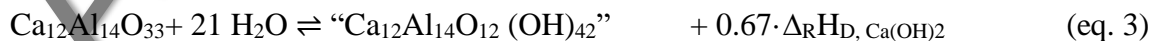
The relative enthalpies of dehydration were calculated by graphical integration of the DSC curves for the active samples, taking the well-known $\Delta_{\text{R}}\text{H}_{\text{Ca}(\text{OH})_2}$ [J/g] as a reference and the results obtained are showed in Table 2. It can be seen that the sample with the highest relative enthalpy of dehydration is the sample prepared at 1000°C (M-1000-A). This is in good agreement with the TG-Results showed in Figure 6 where it can be seen that the Sample M-1000-A is the one with the higher Δ_{mD} (~27 wt%), hence a greater amount of water is involved in the dehydration reaction.

Table 2. Relative enthalpies of hydration and dehydration of activated samples

Sample	$\Delta_{\text{R}}\text{H}_{1\text{D}, \text{Mayenite X}} / \Delta_{\text{R}}\text{H}_{1\text{D}, \text{Ca}(\text{OH})_2}$ $p_{\text{H}_2\text{O}} = 0 \text{ kPa}$
M-600-A	0.25
M-800-A	0.45
M-1000-A	0.67

Based on the amount

According to the equation 2 and the Δ_{mD} (~27 wt%) obtained for M-1000-A, the dehydration reaction which took place under these conditions is:



It is important to mention that the hydrated product of the Mayenite material is amorphous

where its XRD Diffractogram shows no peak. However, as no structural refinement of this material is possible, its general formula “Ca₁₂Al₁₄O₁₂ (OH)₄₂” is introduced between quotation marks. Figure 8 shows the XRD diffractograms obtained for the M-1000-A after the 1st and the 10th hydration/dehydration cycles. As it can be observed, both materials show patterns similar to the pristine one which confirms the cyclability of the material where the Mayenite structure was maintained at least after 10 hydration/dehydration cycles. On the other side, the broadening and intensity of the peaks clearly indicate the decrease of the crystallinity of the material when the number of the cycles increases. The decrease in crystallinity also leads to a decrease in chemical conversion over the cycles, as can be seen in the TG signals shown in Figure 9. Therefore, the energy released due to the hydration of the solid phase also lowers over the cycles (See Figure 9, DSC Signals).

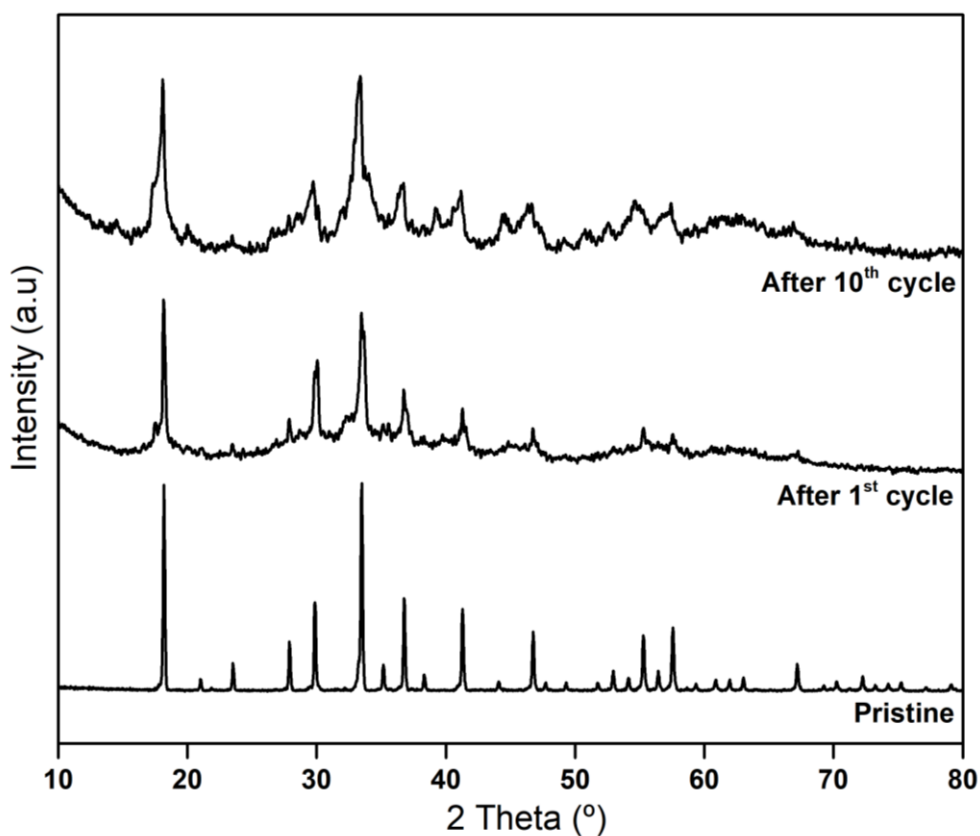


Figure 8. XRD diffractograms of Mayenite, the pristine (bottom) and after the 1st (middle) and 10th (top) hydration-dehydration cycles.

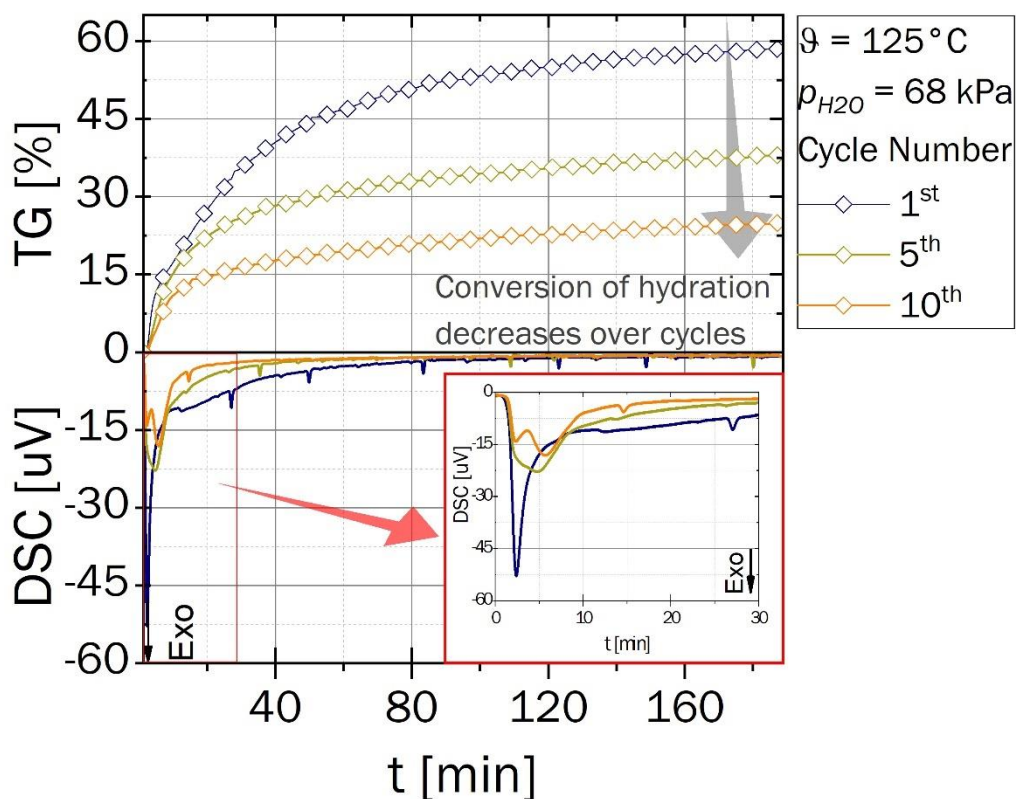


Figure 9 Chemical conversion of re-hydration of M-1000-A over 10 cycles, performed at 125°C and 68 kPa

However, in this work the reaction reversibility was confirmed, while the mitigation of reaction degradation with the cycles is ongoing in our laboratories following two approaches where the first one aims the reactivation of the material after a certain number of cycles and the second one is based on investigating the stabilization of the crystalline structure with some dopants.

4. Conclusions

The preparation of $\text{Ca}_{12}\text{Al}_{14}\text{O}_{33}$ Mayenite structure was successfully performed by using the Evaporation-Induced Self-Assembly (EISA) method. Four oxide samples, i.e. M-600-NA, M800-NA, M-1000-NA and M1100-NA, were obtained by the calcination of the primary reactants at 600, 800, 1000 and 1100 °C. XRD and SEM analyses reveal that the M-600-NA and M800-NA show an amorphous nature without the formation of the mixed structure for the first sample. The samples M-1000-NA and M1100-NA show a good crystallinity with the formation of Mayenite structure. The hydration process of these two materials was very

hard to be conducted at low partial pressures of water vapor (96 kPa). However, a novel activation process of these materials was developed within this work that allows the activation of the sample prepared at 1000 °C, which can be expanded for the activation of other materials that in literature were considered inactive.

The $\text{Ca}_{12}\text{Al}_{14}\text{O}_{33}$ Mayenite exhibits a dehydration process to be transformed to “ $\text{Ca}_{12}\text{Al}_{14}\text{O}_{12}(\text{OH})_{42}$ ” hydroxide at 228 °C with which is much lower compared to $\text{CaO}/\text{Ca}(\text{OH})_2$ pair reaction temperatures between 300 and 500 °C. Furthermore, $\text{Ca}_{12}\text{Al}_{14}\text{O}_{33}/\text{Ca}_{12}\text{Al}_{14}\text{O}_{12}(\text{OH})_{42}$ pair counts with a relative enthalpy of dehydration $0.67 \cdot \Delta_{\text{R}}H_{\text{D, Ca}(\text{OH})_2}$.

Finally, the reaction reversibility of Mayenite was confirmed at least for 10 hydration/dehydration cycles, but on the other side the material crystallinity becomes lower which needs a regeneration step after a certain number of cycles in order to keep the reaction performance.

In particular the low dehydration temperature of 228 °C offers many application possibilities for this storage material. For example current molten salt based CSP-plants operate at a temperature difference between 280 and 560 °C. Consequently the complete temperature difference of the heat transfer fluid could usefully be incorporated into the storage system. Additionally the larger enthalpy of reaction of thermochemical materials leads to less required storage material thus decreasing the cost per kWh of storage capacity. In order to further elaborate the application potential of the material, the reaction should be investigated in lab scale storage reactors under process relevant boundary conditions.

Acknowledgments

The authors acknowledge the financial support from the European Commission through the H2020 program under Grant agreement number 657690. The authors express their sincere thanks to Yagmur Polat and Cristina Luengo for their technical support. The authors would like to thank Andrea Hanke at the DLR-Institute of Engineering Thermodynamics for her technical support.

References:

- [1] T. Yan, R.Z. Wang, T.X. Li, L.W. Wang, I.T. Fred, A review of promising candidate reactions for chemical heat storage, *Renew. Sustain. Energy Rev.* 43 (2015) 13–31. doi:10.1016/j.rser.2014.11.015.
- [2] M. Dincer, I.; Rosen, Thermal energy storage. Systems and applications., John Wiley & Sons, 2002.
- [3] S. Afflerbach, M. Kappes, A. Gipperich, R. Trettin, W. Krumm, Semipermeable encapsulation of calcium hydroxide for thermochemical heat storage solutions, *Sol. Energy.* 148 (2017) 1–11. doi:10.1016/j.solener.2017.03.074.
- [4] S. Tesconi, C. Agrafiotis, S. Breuer, L. De Oliveira, M. Neises-Von Puttkamer, M. Roeb, C. Sattler, Thermochemical solar energy storage via redox oxides: Materials and reactor/heat exchanger concepts, *Energy Procedia.* 49 (2013) 1034–1043. doi:10.1016/j.egypro.2014.03.111.
- [5] J. Cot-Gores, A. Castell, L.F. Cabeza, Thermochemical energy storage and conversion: A state-of-the-art review of the experimental research under practical conditions, *Renew. Sustain. Energy Rev.* 16 (2012) 5207–5224. doi:10.1016/j.rser.2012.04.007.
- [6] G. Karagiannakis, C. Pagkoura, A. Zygogianni, S. Lorentzou, A.G. Konstandopoulos, Monolithic Ceramic Redox Materials for Thermochemical Heat Storage Applications in CSP Plants, *Energy Procedia.* 49 (2014) 820–829. doi:10.1016/j.egypro.2014.03.089.
- [7] A.J. Carrillo, D.P. Serrano, P. Pizarro, J.M. Coronado, Thermochemical heat storage based on the Mn_2O_3/Mn_3O_4 redox couple: influence of the initial particle size on the morphological evolution and cyclability, *J. Mater. Chem. A.* 2 (2014) 19435–19443. doi:10.1039/C4TA03409K.
- [8] A.J. Carrillo, D.P. Serrano, P. Pizarro, J.M. Coronado, Thermochemical heat storage at high temperatures using Mn_2O_3/Mn_3O_4 system: Narrowing the redox hysteresis by metal co-doping, *Energy Procedia.* 73 (2015) 263–271. doi:10.1016/j.egypro.2015.07.686.
- [9] L. André, S. Abanades, Evaluation and performances comparison of calcium, strontium and barium carbonates during calcination/carbonation reactions for solar thermochemical energy storage, *J. Energy Storage.* 13 (2017) 193–205. doi:10.1016/j.est.2017.07.014.
- [10] E. Bagherisereshki, J. Tran, F. Lei, N. AuYeung, Investigation into $SrO/SrCO_3$ for high temperature thermochemical energy storage, *Sol. Energy.* 160 (2018) 85–93. doi:10.1016/j.solener.2017.11.073.
- [11] K.G. Sakellariou, G. Karagiannakis, Y.A. Criado, A.G. Konstandopoulos, Calcium oxide based materials for thermochemical heat storage in concentrated solar power plants, *Sol. Energy.* 122 (2015) 215–230. doi:10.1016/j.solener.2015.08.011.

- [12] F. Schaube, A. Kohzer, J. Schütz, A. Wörner, H. Müller-Steinhagen, De- and rehydration of $\text{Ca}(\text{OH})_2$ in a reactor with direct heat transfer for thermo-chemical heat storage. Part A: Experimental results, *Chem. Eng. Res. Des.* 91 (2013) 856–864. doi:10.1016/j.cherd.2012.09.020.
- [13] F. Schaube, I. Utz, A. Wörner, H. Müller-Steinhagen, De- and rehydration of $\text{Ca}(\text{OH})_2$ in a reactor with direct heat transfer for thermo-chemical heat storage. Part B: Validation of model, *Chem. Eng. Res. Des.* 91 (2013) 865–873. doi:10.1016/j.cherd.2013.02.019.
- [14] P. Pardo, A. Deydier, Z. Anxionnaz-Minvielle, S. Rougé, M. Cabassud, P. Cognet, A review on high temperature thermochemical heat energy storage, *Renew. Sustain. Energy Rev.* 32 (2014) 591–610. doi:10.1016/j.rser.2013.12.014.
- [15] S. Tescari, C. Agrafiotis, S. Breuer, L. De Oliveira, M. Neises-Von Puttkamer, M. Roeb, C. Sattler, Thermochemical solar energy storage via redox oxides: Materials and reactor/heat exchanger concepts, *Energy Procedia.* 49 (2013) 1034–1043. doi:10.1016/j.egypro.2014.03.111.
- [16] E. Alonso, C. Pérez-Rábago, J. Licurgo, E. Fuentealba, C.A. Estrada, First experimental studies of solar redox reactions of copper oxides for thermochemical energy storage, *Sol. Energy.* 115 (2015) 297–305. doi:10.1016/j.solener.2015.03.005.
- [17] M.N. Azpiazu, J.M. Morquillas, A. Vazquez, Heat recovery from a thermal energy storage based on the $\text{Ca}(\text{OH})_2/\text{CaO}$ cycle, *Appl. Therm. Eng.* 23 (2003) 733–741. doi:10.1016/S1359-4311(03)00015-2.
- [18] F. Schaube, L. Koch, A. Wörner, H. Müller-Steinhagen, A thermodynamic and kinetic study of the de- and rehydration of $\text{Ca}(\text{OH})_2$ at high H_2O partial pressures for thermo-chemical heat storage, *Thermochim. Acta.* 538 (2012) 9–20. doi:10.1016/j.tca.2012.03.003.
- [19] T. Nagel, H. Shao, C. Roßkopf, M. Linder, A. Wörner, O. Kolditz, The influence of gas-solid reaction kinetics in models of thermochemical heat storage under monotonic and cyclic loading, *Appl. Energy.* 136 (2014) 289–302. doi:10.1016/j.apenergy.2014.08.104.
- [20] M. Schmidt, M. Linder, Power generation based on the $\text{Ca}(\text{OH})_2/\text{CaO}$ thermochemical storage system – Experimental investigation of discharge operation modes in lab scale and corresponding conceptual process design, *Appl. Energy.* 203 (2017) 594–607. doi:10.1016/j.apenergy.2017.06.063.
- [21] C. Roßkopf, M. Haas, A. Faik, M. Linder, A. Wörner, Improving powder bed properties for thermochemical storage by adding nanoparticles, *Energy Convers. Manag.* 86 (2014) 93–98. doi:10.1016/j.enconman.2014.05.017.
- [22] M. Schmidt, C. Szczukowski, C. Roßkopf, M. Linder, A. Wörner, Experimental results of a 10 kW high temperature thermochemical storage reactor based on calcium hydroxide, *Appl. Therm. Eng.* 62 (2014) 553–559.

doi:10.1016/j.applthermaleng.2013.09.020.

- [23] M. Schmidt, A. Gutierrez, M. Linder, Thermochemical energy storage with CaO/Ca(OH)₂– Experimental investigation of the thermal capability at low vapor pressures in a lab scale reactor, *Appl. Energy*. 188 (2017) 672–681. doi:10.1016/j.apenergy.2016.11.023.
- [24] A. Shkatulov, J. Ryu, Y. Kato, Y. Aristov, Composite material “Mg(OH)₂/vermiculite”: A promising new candidate for storage of middle temperature heat, *Energy*. 44 (2012) 1028–1034. doi:10.1016/j.energy.2012.04.045.
- [25] D.-K. Lee, L. Kogel, S.G. Ebbinghaus, I. Valov, H.-D. Wiemhoefer, M. Lerch, J. Janek, Defect chemistry of the cage compound, Ca₁₂Al₁₄O_{33-δ}—understanding the route from a solid electrolyte to a semiconductor and electride, *Phys. Chem. Chem. Phys.* 11 (2009) 3105–3114. doi:10.1039/B818474G.
- [26] Brinker, C.J., Lu, Y., Sellinger, A. and Fan, H. (1999), Evaporation-Induced Self-Assembly: Nanostructures Made Easy. *Adv. Mater.*, 11, (1999) 579–585. doi:10.1002/(SICI)1521-4095(199905)11.
- [27] J. Rodríguez-Carvajal, Recent advances in magnetic structure determination by neutron powder diffraction, *Phys. B Condens. Matter*. 192 (1993) 55–69. doi:10.1016/0921-4526(93)90108-I.
- [28] L. Palacios, A. Ngeles, G. De, L. Torre, S. Bruque, J.L. García-Muñoz, S. García-Granda, D. Sheptyakov, M. a G. Aranda, Crystal Structures and in-Situ Formation Study of Mayenite Electrides, *Inorg. Chem.* 46 (2007) 409–416. doi:10.1021/ic0700497.
- [29] K. Hayashi, M. Hirano, S. Matsuishi, H. Hosono, Microporous Crystal 12CaO · 7Al₂O₃ Encaging Abundant O⁻ Radicals, 124 (2002) 738–739. DOI: 10.1021/ja016112n
- [30] J.E. Medvedeva, A.J. Freeman, Hopping versus bulk conductivity in transparent oxides : 12 Ca O · 7 Al₂ O₃ Hopping versus bulk conductivity in transparent oxides : 12CaO · 7Al₂O₃, 955 (2013) 10–13. doi:10.1063/1.1781362.
- [31] H. Boysen, I. Kaiser-bischoff, M. Lerch, Anion Diffusion Processes in O- and N-Mayenite Investigated by Neutron Powder Diffraction, 8 (2008) 5–6. ISSN 1862-4138
- [32] S.W. Kim, S. Matsuishi, T. Nomura, Y. Kubota, M. Takata, K. Hayashi, T. Kamiya, M. Hirano, Metallic State in a Lime – Alumina Compound with Nanoporous Structure, *Nano Letters* (2007) 7 (5), 1138-1143
- DOI: 10.1021/nl062717b [33] Y. Wang, M.D. LeVan, Adsorption Equilibrium of Binary Mixtures of Carbon Dioxide and Water Vapor on Zeolites 5A and 13X, *J. Chem. Eng. Data*. 55 (2010) 3189–3195. doi:10.1021/je100053g.